Thermally stimulated capacitance in gamma irradiated epitaxial 4H-SiC Schottky barrier diodes

P. Vigneshwara Raja[1] and N. V. L. Narasimha Murty[2,a)]
[1]*Micro-Fabrication and Characterization Lab, School of Electrical Sciences, IIT Bhubaneswar, Odisha 752050, India*
[2]*Electrical Engineering, IIT Tirupati, Tirupati, Andhra Pradesh 517506, India*

(Received 2 September 2017; accepted 7 November 2017; published online 4 December 2017)

Deep level defects in 4H-SiC Schottky barrier diodes (SBDs) fabricated on n-type epitaxial 4H-SiC have been identified by thermally stimulated capacitance (TSCAP) spectroscopy prior to and after ^{60}Co-gamma irradiation. The TSCAP measurements on the non-irradiated SBDs reveal two electron traps at E_c-0.63 eV (~250 K) and E_c-1.13 eV (~525 K), whereas only one trap at E_c-0.63 eV is identified by conventional thermally stimulated current (TSC) measurements. Hence, TSCAP spectroscopy is more effective in identifying deep level defects in epitaxial 4 H-SiC SBDs as compared to the TSC spectroscopy. Upon exposure to ^{60}Co-gamma rays up to a dose of 100 Mrad, significant changes in the concentration of the traps at E_c-0.63 eV, E_c-1.13 eV, and one new trap at E_c-0.89 eV (~420 K) are observed. The electrical characteristics of the SBDs are considerably changed after gamma irradiation. The dominant mechanisms responsible for the irradiation induced changes in the SBD electrical characteristics are analyzed by incorporating the trap signatures in the commercial Silvaco® TCAD device simulator. The extracted trap parameters of the irradiated SBDs may be helpful in predicting the survival of 4H-SiC SBD detectors at higher irradiation levels. *Published by AIP Publishing*. https://doi.org/10.1063/1.5003068

I. INTRODUCTION

Silicon carbide (SiC) detectors are recommended for radiation detection in space applications.[1–3] For employing SiC detectors in these kinds of applications, radiation detection capabilities of detectors on epitaxial 4H-SiC (polytype of SiC) were being investigated for the past ten years.[3–7] The 4H-SiC detectors can be a potential alternative for the widely used silicon detectors for astronomical imaging systems.[3] The most important issue to develop the detection systems for the space applications is the reliability of the detectors upon exposure to high-energy radiations such as gamma rays.[8] After the gamma irradiation, the detector performance is degraded by the irradiation induced defects in the detector material.[9] Hence, the gamma irradiation produced traps in 4H-SiC need to be studied. Therefore, this work is targeted to identify the deep level traps in the gamma irradiated epitaxial 4H-SiC.

Gamma irradiation effects on 4H-SiC diodes have been extensively studied in the literature. On the other hand, very few works are available on characterizing the gamma irradiation induced defects in the 4H-SiC. Recently, Miyazaki *et al.*[10] reported the ^{60}Co-gamma irradiation induced deep level defects in the epitaxial 4H-SiC MOS capacitors identified by deep level transient spectroscopy (DLTS). The authors observed the elimination of the basal plane dislocation (BPD) crystal defects at the gamma dose of 100 Mrad from the photoluminescence (PL) spectra. In addition, the authors considered that the BPD defect was possibly transformed into threading edge dislocation and stacking faults at 100 Mrad. However, the changes in the electrical properties of the device are not reported. For this reason, the current work is focused to study the ^{60}Co-gamma irradiation effects on the n-type epitaxial 4H-SiC Schottky barrier diodes (SBDs) up to a dose of 100 Mrad. As the reports are sparse in the literature, further studies are needed to get more information about the gamma induced traps in the n-type epitaxial 4H-SiC. Therefore, the ^{60}Co-gamma irradiation induced defects in epitaxial 4H-SiC SBDs are identified in this work.

Traps in the SBDs can be determined by thermally stimulated current[11] and capacitance[12] (TSC and TSCAP) measurements. Extensive studies have been carried out to identify the traps in as-grown[12–20] and irradiated[4,10,21–25] 4H-SiC epilayers by using DLTS technique. Whereas, in the literature, TSCAP technique has been employed by Menichelli *et al.*[12] to identify the traps in the epitaxial 4H-SiC p^+-n diodes, and even here also the DLTS is emphasized. The main advantage of the TSC and TSCAP methods is their simple measurement setup compared to DLTS. Moreover, the TSC technique can be applicable for characterizing defects in junction devices like SBDs,[11] high resistivity bulk devices,[26] and heavily irradiated devices[27] (even in case of $N_T \gg N_{eff}$). Nevertheless, the TSC signal is affected by the device leakage current at higher temperatures.[11,26] On the other hand, the TSCAP technique can be able to differentiate the electron and hole traps in the sample and the signal sensitivity is not affected by the device leakage current.[28–30] In this work, traps in the 4H-SiC SBDs are characterized by TSCAP spectroscopy. From the results, the sensitivity and effectiveness of the TSCAP technique for identifying the defects in the epitaxial 4H-SiC are compared with the DLTS. The current work may provide some new information about the gamma irradiation

a)Author to whom correspondence should be addressed: nnmurty@iittp.ac.in.

induced traps in 4H-SiC epilayers. Furthermore, the changes in the electrical characteristics of the SBDs after irradiation are investigated by incorporating the irradiation produced traps in the commercial Silvaco® TCAD device simulator.

II. EXPERIMENT

The n-type epitaxial 4H-SiC wafers from CREE, Inc., were used for the SBD fabrication. The wafers have a 30 μm thick, low nitrogen doped (with a concentration of $5 \times 10^{14}\,cm^{-3}$) epitaxial layer with a low micropipe density of $\leq 15\,cm^{-2}$, grown on 364 μm thick highly doped ($\sim 10^{18}\,cm^{-3}$) n-type 4H-SiC substrate.

A. 4H-SiC SBD fabrication

The SBDs were fabricated at CSIR-CEERI, Pilani, India. The 4H-SiC wafers were first diced, and the samples were effectively cleaned as per the degreasing and RCA cleaning procedure.[31] Two types of 4H-SiC SBDs (Ni/4H-SiC SBDs and Ti/4H-SiC SBDs) were fabricated. For the fabrication of Ni/4H-SiC SBDs, Schottky contacts were formed by the sputtering of Ni (200 nm) through a shadow mask on the Si-face of the 4H-SiC, whereas the Ti (50 nm)/Au (150 nm) bi-layer was considered as a Schottky contact for the Ti/4H-SiC SBDs. In both the SBDs, the Ti/Au bi-layer combination was sputtered on the C-face of the 4H-SiC for Ohmic contact. Since the as-deposited Ti can form Ohmic contact[32,33] with the n^+-4H-SiC substrate ($\sim 10^{18}\,cm^{-3}$) and with a low specific contact resistivity[33] (SCR) of $\sim 2.3 \times 10^{-3}\,\Omega\,cm^2$, no thermal annealing was carried out after forming contacts on the samples. Each processed sample consists of an array of SBDs with two different active areas 3.8 mm^2 and 1.8 mm^2.

B. TSC and TSCAP measurements

At first, the I-V and C-V measurements of SBDs were carried out by using Agilent B1500A Semiconductor Device Analyzer at room temperature. The schematic view of the TSC/TSCAP measurement setup is shown in Fig. 1. The TSC and TSCAP experiments were conducted in the temperature range of 80 K–675 K under vacuum $<10^{-6}$ Torr using the Janis® cryogenic probe station connected to the Lakeshore 336 temperature controller. For current and capacitance measurements, Keithley 6517B Electrometer and Agilent 4285A LCR meter are interfaced with the probe station. In TSC measurements, the samples were initially cooled to a low temperature ($\sim$80 K), and then traps in the samples were filled by 2 mA current injection for 100 s. Finally, the samples were heated at a constant rate under the reverse bias of −100 V and the thermal emission current was recorded with respect to the temperature (i.e., TSC spectrum) in the LabVIEW interfaced PC. Three different heating rates (0.08 K/s, 0.12 K/s, and 0.16 K/s) were considered in TSC measurements for extracting the trap activation energies using the variable heating rate method.[11,26]

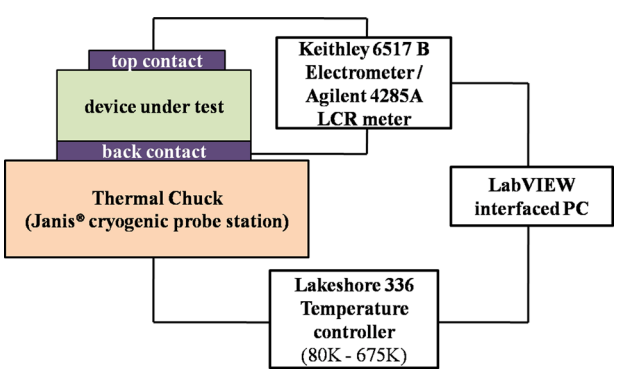

FIG. 1. Schematic view of the TSC/TSCAP measurement setup.

TSCAP characterization was performed at a signal frequency of 1 MHz and with a small AC signal of 30 mV. At the high signal frequency of 1 MHz, the AC signal applied to the SBD does not affect the occupancy of the deep traps; hence, the emission probability of the occupied deep traps mainly depends on the sample temperature.[29,30] For identifying the traps in the samples, TSCAP spectra without and with trap filling were taken. For acquiring the TSCAP spectra without trap filling, the samples were heated up to 675 K from room temperature; subsequently, they were cooled from 675 K to T_0 (120–160 K) under the reverse bias voltage of −40 V for completely emptying the traps within the space charge region. Upon reaching T_0, the samples were heated at 0.12 K/s under −40 V without any trap filling and the changes in the capacitance were measured with respect to the sample temperature. For obtaining the TSCAP spectra with trap filling, the sample cooling procedure mentioned earlier was followed with the 2 mA current injection at T_0. In some samples, the TSCAP spectrum with trap filling was acquired for the two conditions, viz., sample cooling with and without bias voltage (−40 V), to identify the metastable[34–36] defects (one charge state can exist more than one configuration) in the 4H-SiC epitaxial layer. To check the sensitivity of the TSCAP measurements with the heating rate, some TSCAP spectra were obtained for the three different heating rates of 0.08 K/s, 0.12 K/s, and 0.16 K/s.

C. Gamma irradiation details

The gamma irradiation of the 4H-SiC SBDs was carried out by using ^{60}Co-gamma source at UGC-DAE Consortium for Scientific Research (CSR), Kolkata Centre, India. It may be noted that the gamma irradiations were performed on the fabricated SBDs (i.e., after the metal depositions). The samples were placed close to the ^{60}Co-gamma source at a location where the received dose rate was about 0.25 Mrad/h, as calculated by using the Fricke dosimetry system. The samples were continuously exposed to the ^{60}Co-gamma rays for the irradiation period of 400 h to obtain the dose of 100 Mrad. The electrical characteristics and TSCAP spectra of the gamma irradiated SBDs were measured.

III. SIMULATION SETUP

The simulations are performed in the commercially available Silvaco TCAD device simulator[37,38] at the temperature of 300 K. Figure 2 shows the typical 2D-structure of the SBD generated by the Silvaco ATHENA process simulation.[37] The generated SBD structure is then loaded into the

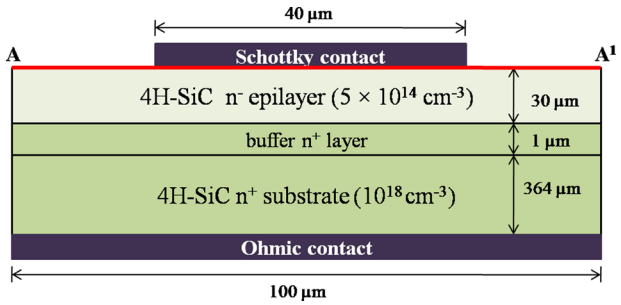

FIG. 2. 2D-structure of the 4H-SiC SBD considered in simulation.

Silvaco ATLAS device simulator.[38] The 4H-SiC material parameters and the physical models[38] [Shockley–Read–Hall (SRH) recombination, Auger recombination, Fermi-Dirac carrier statistics, field-dependent carrier mobility, and bandgap narrowing] are carefully selected in the simulation. Particularly, a special attention is given to the Schottky contact models. The work function (W) for the Schottky contact is chosen in the device simulator as follows:[38]

$$W = \chi + \Phi_B, \tag{1}$$

where χ is the electron affinity of 4H-SiC, and Φ_B is the Schottky barrier height. The Schottky barrier height (Φ_B) extracted from the I-V measurements is taken for the Schottky contact model. Accordingly, the work function specified top contact (Ni or Ti) act as a Schottky contact and the undefined bottom contact (Ti) by default is considered as Ohmic. Hence, in Ni/4H-SiC SBD structure, Ni is utilized for Schottky contact with a length of 40 μm and Ti is used for Ohmic contact. On the other hand, Ti is considered as Schottky and Ohmic contacts for the simulated structure of the Ti/4H-SiC SBD.

The SBD reverse current density (J_R) due to the thermionic emission along with the Schottky barrier lowering $(\Delta\Phi_B)$, and the tunneling effects may be written as[39,40]

$$J_R = A^* T^2 e^{-(\Phi_B - \Delta\Phi_B)/kT} e^{C_T E_m^2}, \tag{2}$$

where A^* is the Richardson's constant, T is the temperature, k is the Boltzmann's constant, C_T is the tunneling coefficient, and E_m is the electric field at the metal-semiconductor interface of the SBD. The Schottky barrier lowering is directly proportional to $\sqrt{E_m}$, while the tunneling current density is proportional to the E_m^2.[39] Therefore, both the Schottky barrier lowering effect and the parabolic Schottky field emission models (for accounting the tunneling current) are incorporated to predict the reverse I-V characteristics.[38] Furthermore, anisotropic carrier mobility and impact ionization[38] are selected for modeling the anisotropic physical properties of the 4H-SiC.

The traps identified in the non-irradiated SBDs from the measurements are added in the physical model to investigate the effects of defects on the electrical properties of the virgin SBDs. Traps are considered as acceptor-like defects. The electron capture cross section of the defects determined from the measurements is taken in the physical model. The change in the effective space charge of the SBD due to the traps is accounted in the model as[38]

$$div(\varepsilon\Delta\Psi) = -\rho - Q_T, \tag{3}$$

where Ψ is the electrostatic potential, ε is the permittivity of 4H-SiC, ρ is the local space charge density, and Q_T is total charge density introduced by the traps. The trap assisted tunneling and the Poole-Frenkel barrier lowering effects are also accounted in the simulation.[38] Note that, the used-defined parameters of Schottky barrier effect, parabolic field emission, SRH recombination, auger recombination, and anisotropic carrier mobility models are tuned to validate the pre-irradiation simulation characteristics with our experimental data. Moreover, the hole capture cross section of the traps is assumed in the model. The main motive of the simulation is to identify the physical mechanisms behind the observed changes in the SBD characteristics after gamma irradiation. To study the same, the gamma irradiation induced defects (i.e., radiation damage model) are included and the irradiation induced changes in the electrical characteristics are investigated.

IV. RESULTS AND DISCUSSION

A. Pre-irradiation electrical characteristics

The Schottky barrier height of Ni/4H-SiC and Ti/4H-SiC SBDs (calculated[41] from the forward I-V characteristics) is found to be 1.21 eV and 1.12 eV, respectively. The leakage current density of Ni/4H-SiC and Ti/4H-SiC SBDs is noted as 3.3 nA/cm^2 (at -100 V) and 5.6 nA/cm^2 (at -100 V). The effective doping concentration ($\sim 5 \times 10^{14}$ cm^{-3}) of the 4H-SiC epilayer is determined[41] from the (1/C)^2-V characteristics at a signal frequency of 1 MHz.

B. Traps in non-irradiated SBDs

Figure 3 shows the TSC spectrum obtained with the Ni/4H-SiC SBD (1.8 mm^2) at the heating rate of 0.12 K/s. A single TSC peak (P1) at $\sim$250 K is observed. The SBD leakage current is considerably increased after $\sim$280 K; hence no TSC peaks are noticeable beyond this temperature. Some SBDs have not given any TSC peaks in the entire temperature range due to the excessive leakage currents. Therefore,

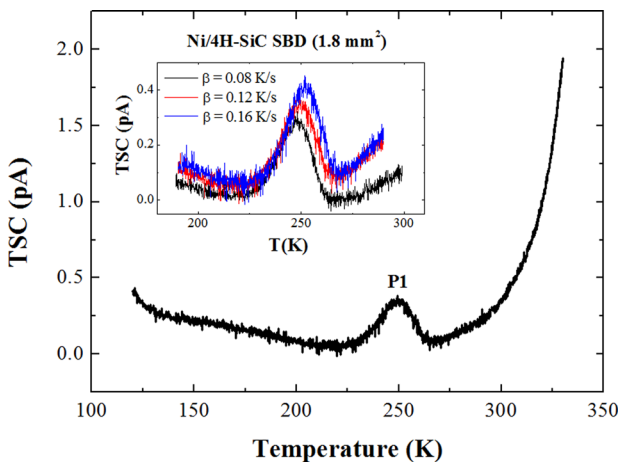

FIG. 3. TSC spectrum obtained with Ni/4H-SiC SBD (1.8 mm^2) at the heating rate of 0.12 K/s. The inset shows the TSC spectra for different heating rates.

the TSC measurements conducted on the SBD are limited by the leakage current. The thermally stimulated current (I_{TSC}) measured in the SBD from a trap level during the temperature ramp up is given by[42,43]

$$I_{TSC} = \frac{qAd}{2} X N_T \exp\left(-\int_{To}^{T} \frac{X}{\beta} dT\right), \tag{4}$$

where A is the SBD active area, d is the depletion region thickness, N_T is the trap concentration at T_0, β is the heating rate, and X is the carrier thermal emission rate.[26] The magnitude and the peak maximum temperature of the TSC peak P1 is found to increase with the heating rate[11,26] as noticed from the inset of Fig. 3 due to the time-dependent thermal emission rate[30] of the carriers as per the Eq. (4). The peak maximum temperature of P1 is noted for the different heating rates of 0.08 K/s, 0.12 K/s, and 0.16 K/s and the activation energy of ~0.63 eV is determined from the variable heating rate method.[11,26] The trap concentration of $\sim 2 \times 10^{13}\,\mathrm{cm}^{-3}$ is estimated by the Forbes-Sah method.[42,43] The capture cross section of 5×10^{-16} cm^2 is predicted by fitting[11,26] the numerically simulated spectrum obtained based on the TSC Eq. (4) with the measured peak P1. Note that the trap type (i.e., electron/hole) is not identified from the TSC spectroscopy.

Figure 4 shows TSCAP spectra measured in the Ni/4H-SiC SBD (3.8 mm^2) and the inset shows the TSCAP for different heating rates. In the TSCAP spectrum obtained without trap filling, the depletion capacitance of the SBD is found to increase with the temperature due to the decrease in the built-in voltage.[28] From the TSCAP spectrum obtained with trap filling, two TSCAP steps (i.e., abrupt increase in TSCAP) are observed in the temperature range of 225–265 K (P1) and 490–540 K (P2), respectively. The TSCAP steps (P1 and P2) are generated by the electron traps in the SBD,[28–30] which are explained as follows: Before the trap filling, the SBD depletion capacitance is essentially determined by the ionized donors in the space charge region. After the trap filling at T_0, the ionized donors can be

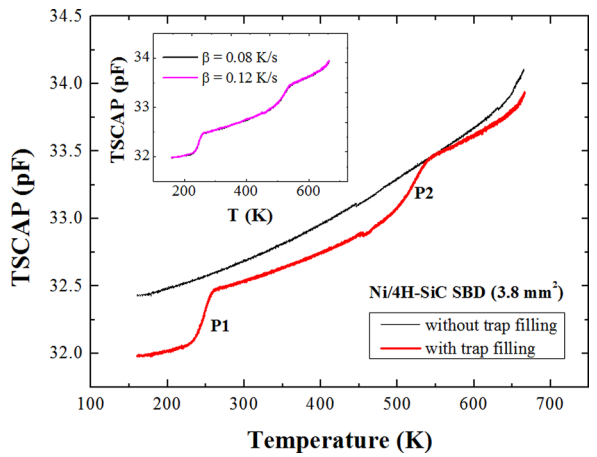

FIG. 4. TSCAP spectrum measured in the Ni/4H-SiC SBD (3.8 mm^2). The inset shows TSCAP for different heating rates.

compensated by the trapped electrons (n_T) in the depletion region, which decreases the capacitance (C) as realized by[28]

$$C = A\sqrt{\frac{q\varepsilon(N_D^+ - n_T)}{2(V_R + V_{bi})}}, \tag{5}$$

where q is the elementary charge, N_D^+ is the ionized donor density in the space charge region, V_R is the reverse bias voltage, and V_{bi} is the built-in potential. From a particular temperature during the TSCAP scan, the thermal emission rate of the trapped electrons from the trap level dominates and hence the de-trapped electrons are instantaneously depleted from the space charge region due to the electric field. As a result, a sudden increase in the capacitance is observed from the temperatures of ~225 K and ~490 K. This process continues until all the trapped electrons from the trap level are released. Therefore, the increasing TSCAP steps in our measurements (P1 and P2) must be produced by the electron traps.

Unlike TSC measurements, the traps are identified at higher temperatures as the TSCAP technique is not limited by the leakage current and the trap type is also determined. Hence, from now, TSCAP results are only presented. From the inset of Fig. 4, it is observed that TSCAP steps do not change with the heating rate (unlike TSC) supporting the earlier reported works.[29,30] In the TSCAP measurements, the change in the space charge layer capacitance is directly recorded by measuring the total charge in the depletion layer,[30] similar to Eq. (5) and hence the TSCAP steps are not changed with the heating rate. Furthermore, no considerable variations in the TSCAP signal magnitude/step height have been observed for P1 and P2 in the Ni/4H-SiC SBDs for both the cooling conditions such as with and without bias voltage. The mid-temperature $(T_{1/2})$ of the TSCAP step is related to the trap activation energy (E_T) by[30]

$$E_T = kT_{1/2} \ln\left[\frac{\nu k T_{1/2}}{q(E_T + 2kT_{1/2})}\right], \tag{6}$$

where ν is the escape frequency factor, as expressed by[30,43]

$$\nu = \sigma N_{C/V} V_{th}, \tag{7}$$

where σ is the defect capture cross section, V_{th} is the thermal velocity of carriers, and $N_{C/V}$ is the effective density of states in conduction or valence band for electron or hole traps. Generally, the value of escape frequency factor is assumed to identify the trap activation energy from the TSCAP.[30] As the trap P1 is identified from the TSC spectroscopy, the escape frequency factor calculated from the TSC is considered in Eq. (6). The electron trap detected at ~525 K is also reported by Hemmingsson *et al.*[21,22] using DLTS, accordingly the escape frequency factor of the trap P2 is chosen based on these works. As a result, the energy level of the traps P1, and P2 is found to be E_c-0.63 eV, and E_c-1.13 eV, respectively. The trap concentration (N_T) is estimated by[28–30]

$$N_T = \frac{2\Delta C}{C_1} N_d = \frac{2(C_2 - C_1)}{C_1} N_d, \tag{8}$$

where C_1 and C_2 are the capacitances at the step starting temperature and the step ending temperature. After investigating all the samples, the trap densities for P1 and P2 are found to be (1–1.5) $\times$ 10^{13} cm^{-3} and (1.2–1.5) $\times$ 10^{13} cm^{-3} from the TSCAP spectroscopy. Note that the trap concentration for P1 identified from TSCAP is slightly lower than that determined from the TSC measurement ($\sim 2 \times 10^{13}$ cm^{-3}); the observed minor variation in the trap concentration may be due to the spatial sensitivity of these measurements.[30] In principle, the sensitivity of the TSCAP signal in the SBDs varies linearly from zero at the junction to a maximum at the outer edge region of the depletion region, whereas the TSC signal sensitivity to the trapped electrons in the n-type substrate is exactly the opposite of the TSCAP.

The TSCAP spectrum acquired for Ti/4H-SiC SBDs is shown in Fig. 5. The spectrum reveals only one trap (P1) and no traces of trap P2. In addition, the trap P2 has not been identified in the Ti/4H-SiC SBDs for the both cooling conditions. It is also noticed from the inset of Fig. 5 that the TSCAP steps are not changed with the heating rate. The P1 trap concentration in the Ti/4H-SiC SBDs is also in the same range of (1–1.5) $\times$ 10^{13} cm^{-3}.

The trap P1 is observed in all studied SBDs revealing that the E_c-0.63 eV is an omnipresent defect in the 4H-SiC epilayer; thus, the trap P1 might be produced by the lifetime killer acceptor-like defect $Z_{1/2}$ commonly observed in the n-type 4H-SiC epilayers.[14,16–20,36] Hemmingsson *et al.*[44] reported that the trap $Z_{1/2}$ is a negative-U center,[36,44] i.e., it captures two electrons simultaneously overcoming the coulomb repulsion force between the two electrons and emits two electrons at the same time when it gets ionized. So, the measured TSCAP step height/TSC signal peak for $Z_{1/2}$ is exactly twice that of the actual trap concentration of $Z_{1/2}$. Hence, the trap concentrations for $Z_{1/2}$ identified from the TSCAP and TSC measurements are divided by two and the modified concentration values are considered for the simulation. As the trap concentration is about 10^{13} cm^{-3}, the trap P1 might significantly reduce the carrier lifetime ($<10^{-6}$ s) in the 4H-SiC epilayer.[17,36]

The other trap at E_c–1.13 eV (P2) may be related to the intrinsic acceptor-like EH5 (Refs. 21, 22, 34, 35, and 45) center. The current observations create a dilemma that whether the P2 is a bulk trap or an interface trap. Note that the TSCAP measurements are very insensitive to the traps located near to the interface of the SBD;[29,30] as a result the P2 may be a bulk trap. The P2 is only observed in Ni/4H-SiC SBDs, so it may be related to Ni impurity based defect complex. However, the diffusion coefficient of Ni in 4H-SiC is extremely small at room temperature.[36] Beyer *et al.*[34,35] reported the bistable configurations (metastable behavior) of the EH5 defect identified from the variations in the DLTS signal magnitude based on the sample cooling conditions. The authors observed the appearance of the EH5 defect upon cooling with bias voltage and almost disappearance of the EH5 defect when cooling without bias for the same DLTS measurement parameters in the high-energy electron irradiated Ni/4H-SiC SBDs. From our TSCAP measurements, it has been found that the appearance and the TSCAP signal magnitude of the trap P2 (EH5) in the Ni/4H-SiC SBDs do not depend on the cooling procedure performed with and without bias voltage. Moreover, the trap P2 (EH5) has not been observed in the Ti/4H-SiC SBDs for both the cooling conditions. Therefore, the bi-stable behaviour of EH5[34,35] has not been identified in the Ni/4H-SiC SBDs from our TSCAP measurements and the EH5 is not observed in the Ti/4H-SiC SBDs even though the same TSCAP procedure is followed. Hence, the reason for the appearance of the P2 in Ni/4H-SiC SBDs is still unclear from the current measurements; studies are underway to identify the reason.

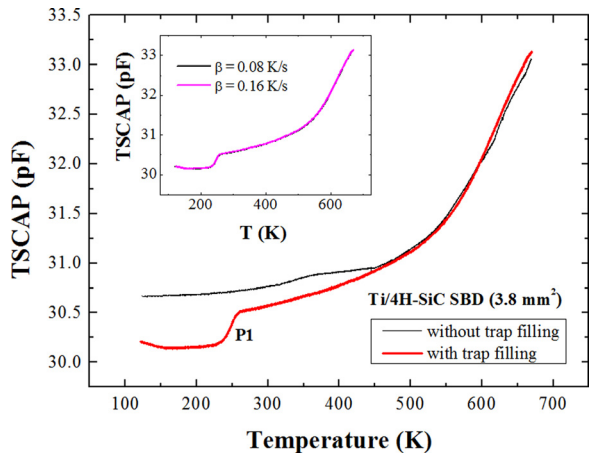

FIG. 5. TSCAP spectrum for the Ti/4H-SiC SBD (3.8 mm^2) and the TSCAP for different heating rates is shown in inset.

The traps identified in the 4H-SiC SBDs are summarized in Table I, along with the trap parameters, such as TSCAP step label, mid-temperature of the TSCAP step ($T_{1/2}$), trap energy location (E_T), trap density (N_T), trap electron capture cross section (σ_n), and trap attribution. Recall that the actual P1 ($Z_{1/2}$) trap concentration (given in Table I) is half of the trap density extracted from the TSCAP/TSC spectroscopy due to the negative-U property.[36,44] The physical structure of the acceptor-like electron trap $Z_{1/2}$ (P1) may be related to the carbon vacancy V_C (2-/0).[36] The possible physical origin of other acceptor-like electron trap EH5 (P2) is a carbon vacancy (V_C) or a carbon interstitial (C_i).[34,35,45] Hence, both the defects are associated with the intrinsic point defects and are acceptor-like states. Recently, Mannan *et al.*[20] identified the same deep level traps such as $Z_{1/2}$ and EH5 in the Ni/4H-SiC SBDs from the DLTS measurements, along with another deep electron trap $EH_{6/7}$ (E_c-1.55 eV). The deep level defects such as $Z_{1/2}$ and $EH_{6/7}$ are commonly observed in the CREE 4H-SiC epilayers,[14,16–20,36] but the trap $EH_{6/7}$ is not detected from our measurements. Note that the TSCAP technique works reasonably well when the defect concentration is quite large i.e., $N_T \geq 0.1N_D$.[29,30] So, it is considered that the trap $EH_{6/7}$ is present in the 4H-SiC epilayer with a low concentration of $<10^{13}$ cm^{-3}. Probably due to this reason, the trap $EH_{6/7}$ is not identified in the TSCAP spectra obtained for 4H-SiC SBDs. The current results suggest that the DLTS is the effective technique for identifying the deep level defects (even accurate for low density traps) in the 4H-SiC SBDs as compared to the TSCAP. However, the TSCAP spectroscopy is suitable for detecting the deep level defects with higher trap concentrations, which might be mainly responsible in

TABLE I. Traps identified in non-irradiated 4H-SiC SBDs by TSC and TSCAP.

Label	$T_{1/2}$ (K)	E_t (eV)	N_t ($\times 10^{13}$ cm^{-3})	σ_n (cm^2)	Possible defects	Possible physical origin	Method used for identification
P1	~250	E_c-0.63	(0.5–1)[a]	$\sim 5 \times 10^{-16}$	$Z_{1/2}$[b]	V_C (2-/0)	TSC, TSCAP
P2	~525	E_c-1.13	(1.2–1.5)	$\sim 2 \times 10^{-18}$	EH5[c]	V_C or C_i	TSCAP

[a]Extracted trap concentrations from TSCAP/TSC divided by two due to negative U property of $Z_{1/2}$.
[b]References 14, 16–20, and 36.
[c]References 21, 22, 34, 35, and 45.

determining the 4H-SiC SBD characteristics by considering their trap concentrations.

C. Traps in gamma irradiated SBDs

Figure 6 shows the TSCAP spectrum obtained with Ni/4H-SiC SBD after ^{60}Co-gamma irradiation. In addition to the traps P1, and P2, one new trap at ~420 K (G420, E_c-0.89 eV) is identified in the gamma irradiated Ni/4H-SiC SBDs. On the other hand, the P1 and G420 are only detected in the gamma irradiated Ti/4H-SiC SBDs, as observed from the Fig. 7. Hence, the P1 and G420 are the omnipresent defects in the ^{60}Co-gamma irradiated 4H-SiC. The concentration of the traps P1, P2, and G420 in the gamma irradiated SBDs is determined as $(1.8–2) \times 10^{14}$ cm^{-3}, $(1.5–1.8) \times 10^{14}$ cm^{-3}, and $(3.8–4) \times 10^{13}$ cm^{-3}, respectively. Hence, the trap density for P1 and P2 is increased by an order of magnitude after gamma irradiation at the dose of 100 Mrad. The gamma irradiation induced defects in the 4H-SiC SBDs are given in Table II. The trap G420 can be assigned to the radiation induced acceptor-like $RD_{1/2}$ center detected in 4H-SiC epilayer.[13,23,46]

The possible physical structure for the trap $RD_{1/2}$ (G420) is one carbon vacancy and one silicon vacancy ($V_C + V_{Si}$) located on adjacent lattice sites.[46] As similar to the interaction mechanism with silicon,[43,47] the ^{60}Co-gamma irradiation creates displacement damage in 4H-SiC possibly through Compton scattered electrons, which produces point defects in the 4H-SiC as suggested by Miyazaki *et al.*[10] After the gamma irradiation, the concentration of the intrinsic acceptor-like traps $Z_{1/2}$ (P1) and EH5 (P2) has been considerably increased in the SBDs together with the creation of new intrinsic acceptor type center $RD_{1/2}$ (G420). Therefore, the ^{60}Co-gamma irradiation may produce intrinsic point defects in the n-type 4H-SiC epitaxial layer and the electronic trap levels introduced within the bandgap by these intrinsic crystal defects may be the acceptor-type traps. Furthermore, it is noted that the traps P1, P2, and G420 are identified in all the studied gamma irradiated Ni/4H-SiC SBDs with the same concentration range. Similarly, the defects P1 and G420 are detected in all investigated Ti/4H-SiC SBDs after gamma irradiation. This may suggest that the gamma irradiation produced defects are uniformly distributed across the 4H-SiC epilayer. However, further physical characterization studies [TEM/SEM/electron beam induced current (EBIC)] are needed to support this conclusion.

D. Gamma irradiation effects on electrical characteristics

In the pre-irradiation simulation model for Ni/4H-SiC SBDs, the trap signatures of P1 and P2 given in Table I are included together with the hole capture cross section of 8×10^{-14} cm^2 (P1), 6×10^{-16} cm^2 (P2). For simulating gamma irradiation induced changes in the electrical characteristics of the Ni/4H-SiC SBDs, the trap G420 (with a hole capture cross section of 9×10^{-16} cm^2) is incorporated in the physical model along with the traps P1 and P2. Similarly, the trap P1 is included in the pre-irradiation simulation model for Ti/4H-SiC SBDs and the traps P1 and G420 are considered in the ^{60}Co-gamma radiation damage model for Ti/4H-SiC SBDs.

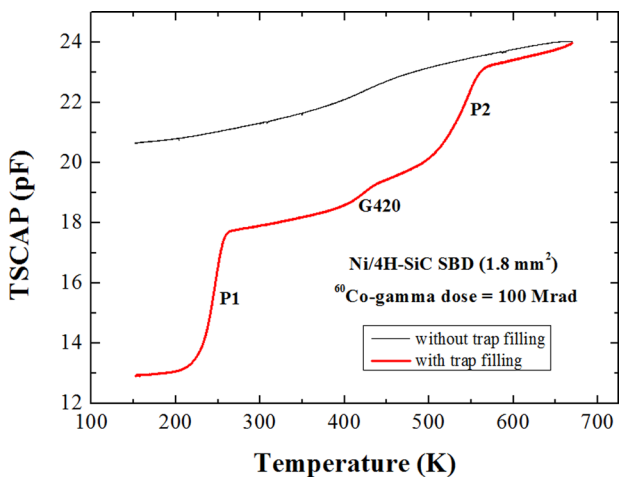

FIG. 6. TSCAP spectrum for the Ni/4H-SiC SBD (1.8 mm^2) after ^{60}Co-gamma irradiation at the dose of 100 Mrad.

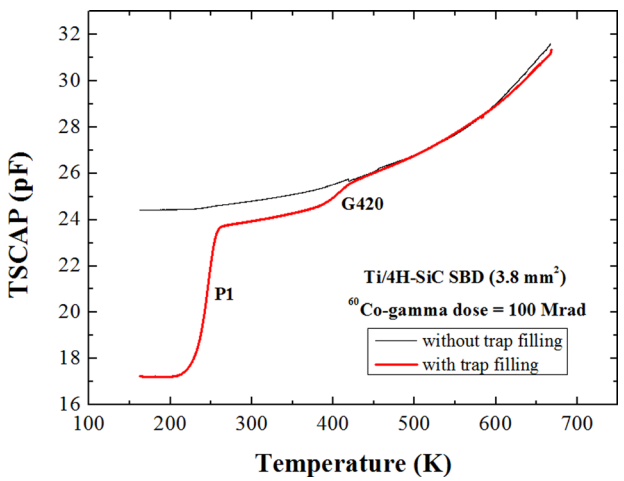

FIG. 7. TSCAP spectrum for the ^{60}Co-gamma irradiated Ti/4H-SiC SBD (3.8 mm^2) at the dose of 100 Mrad.

TABLE II. Traps identified in gamma irradiated 4H-SiC SBDs from TSCAP.

Label	$T_{1/2}$ (K)	E_t (eV)	N_t ($\times 10^{14}$ cm^{-3})	σ_n (cm^2)	Possible defects	Possible physical origin
P1	~250	E_c-0.63	(1.8–2)[a]	$\sim 5 \times 10^{-16}$	$Z_{1/2}$[b]	V_C (2-/0)
P2	~525	E_c-1.13	(1.5–1.8)	$\sim 2 \times 10^{-18}$	EH5[c]	V_C or C_i
G420	~420	E_c-0.89	(0.38–0.4)	$\sim 4 \times 10^{-18}$	$RD_{1/2}$[d]	$V_C + V_{Si}$

[a]Extracted trap concentrations from TSCAP divided by two due to negative U property of $Z_{1/2}$.
[b]References 14, 16–20, and 36.
[c]References 21, 22, 34, 35, and 45.
[d]References 13, 23, and 46.

The measured and simulated ^{60}Co-gamma irradiation induced changes in the reverse leakage current density of the Ni/4H-SiC SBDs are shown in Fig. 8, along with the pre-irradiation data. It is noticed that the simulated reverse leakage current density almost replicates the measured characteristics. The reverse current density of the Ni/4H-SiC SBDs is decreased after the gamma irradiation at the dose of 100 Mrad, in contrary to the irradiation effects observed for the leakage current of the silicon detectors.[9,43,47,48] In the literature, Nava *et al.*[49] and Zhang *et al.*[50] also observed the decrease in the leakage current of the 4H-SiC SBD upon exposure to the ^{60}Co-gamma rays.

The device simulations are also carried out to understand the reverse current conduction mechanism of the 4H-SiC SBDs. The voltage dependence of different components of the reverse leakage current density of the non-irradiated Ni/4H-SiC SBDs obtained through simulations is plotted in Fig. 9. It is noted that the reverse current density without considering the barrier lowering and tunneling is nearly negligible; this current is possibly generated by the thermionic emission and the thermal generation of carriers in the depletion region.[39–41] Even after including the barrier lowering effect, the reverse current density is underestimated by two orders of magnitude. The reverse current density with barrier lowering and tunneling taken into account closely tracks the experimental data, as can be seen from Fig. 9. Hence, the tunneling current is the dominant reverse current conduction mechanism in Ni/4H-SiC SBDs.

Figure 10 shows the simulated electric field (E_m) at the Ni/4H-SiC interface of the SBD obtained along the cutline AA[1] of the Fig. 2. It is noticed that high electric field occurs at the contact edges of the Ni/4H-SiC interface (refer Fig. 2) due to the electric field crowding at the Ni/4H-SiC interface.[39] Therefore, the reverse current density of the 4H-SiC SBDs is mainly governed by the tunneling of electrons from the metal to the semiconductor due to the high electric field at the metal/4H-SiC interface,[39,40] as can be inferred from Fig. 9.

From Fig. 8, it is noted that the reverse leakage current density is decreased after the gamma irradiation at the dose of 100 Mrad. The tunneling current is considerably reduced after gamma irradiation (see Fig. 9), because of the reduction in the electric field at the Ni/4H-SiC interface as seen from

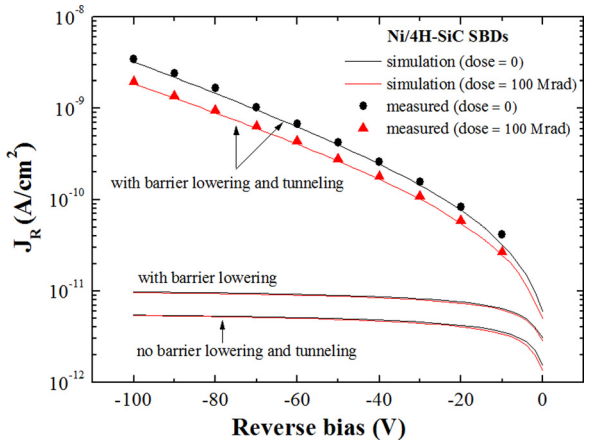

FIG. 9. Simulated ^{60}Co-gamma irradiation effects on different components of the reverse leakage current density of the Ni/4H-SiC SBDs.

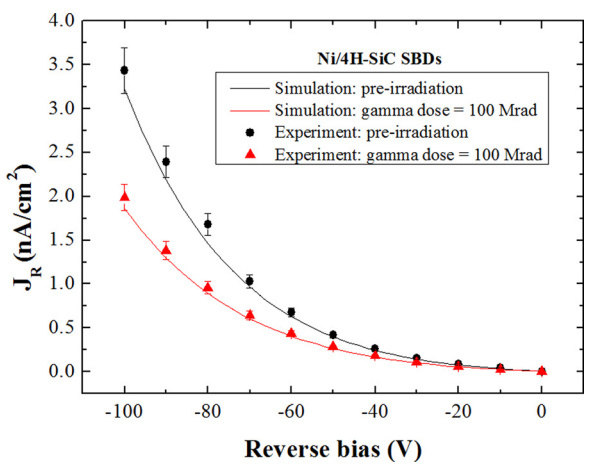

FIG. 8. Measured and simulated reverse current density (J_R) vs. bias voltage (V_R) of Ni/4H-SiC SBDs before and after the ^{60}Co-gamma irradiation.

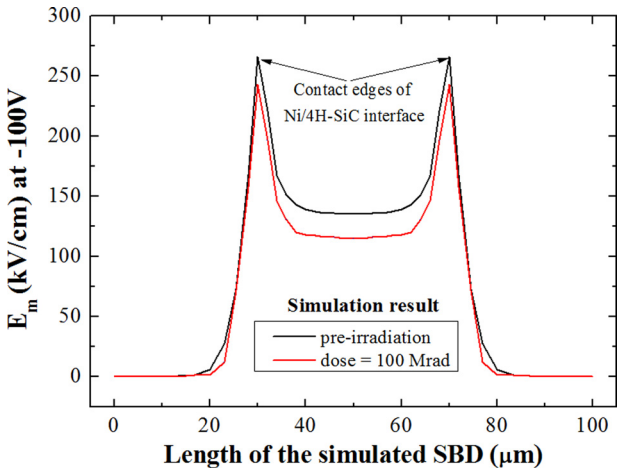

FIG. 10. Simulation of the electric field (at −100 V) at the Ni/4H-SiC interface of the SBD before and after the ^{60}Co-gamma irradiation.

the Fig. 10. For this cause, the Schottky barrier lowering current component is also decreased as noticed from Fig. 9. Hence, the decrease in the leakage current density after gamma irradiation is mainly due to the reduction in the tunneling current.

The measured and simulated changes in the J_R-V_R characteristics of Ti/4H-SiC SBDs are shown in Fig. 11. Similar to the Ni/4H-SiC SBDs, the tunneling current component is the dominant reverse current conduction mechanism in the Ti/4H-SiC SBDs, as identified from the simulations. From Fig. 11, it is observed that the reverse leakage current density is decreased after the gamma irradiation due to the reduction in the tunneling current; but the change in the leakage current density from its initial value is found to be lesser as compared to the Ni/4H-SiC SBDs (compare Figs. 8 and 11). This small change in the leakage current density is because of the absence of the trap P2 in the Ti/4H-SiC SBDs, as found from simulations. Since the energy location of the trap P2 is deep in the bandgap and its concentration is in $10^{14}\,cm^{-3}$ ranges, the trap P2 has shown a considerable impact on change in the reverse current density of the Ni/4H-SiC SBDs.

Figure 12 shows the measured and simulated ^{60}Co-gamma irradiation induced changes in the $(1/C^2)$-V characteristics of the Ni/4H-SiC SBDs. After the gamma irradiation, the effective doping concentration is decreased to $3.8 \times 10^{14}\,cm^{-3}$ from its pre-irradiation value of $5 \times 10^{14}\,cm^{-3}$, because of the compensation of the positive space charge of the ionized donors by the acceptor-like defects introduced negative space charge,[51] as per the Eq. (3). This confirms that the gamma irradiation produced traps in the SBDs are acceptor-like defects and also validates the simulation model. Due to the considerable increase in the concentration of the acceptor-like defects at the dose of 100 Mrad (refer Table II), the decrease in the effective doping concentration is obtained after gamma irradiation. The effective doping concentration (N_{eff}) is related to the electric field at the metal/semiconductor interface of the SBD (E_m) by[39,41]

$$E_m = \sqrt{\frac{2qN_{eff}(V_R + V_{bi})}{\varepsilon}}. \tag{9}$$

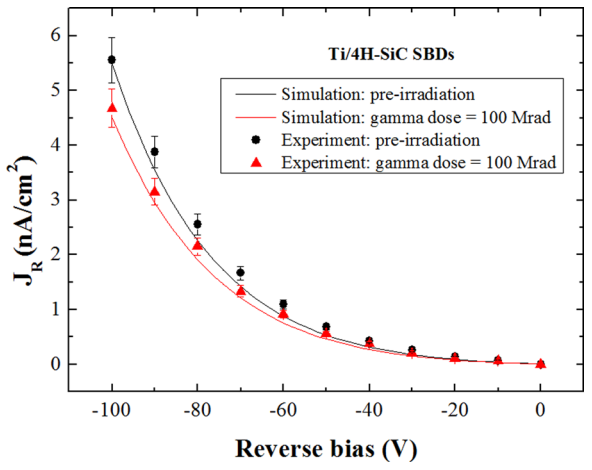

FIG. 11. Measured and simulated ^{60}Co-gamma irradiation induced changes in the J_R-V_R characteristics of the Ti/4H-SiC SBDs.

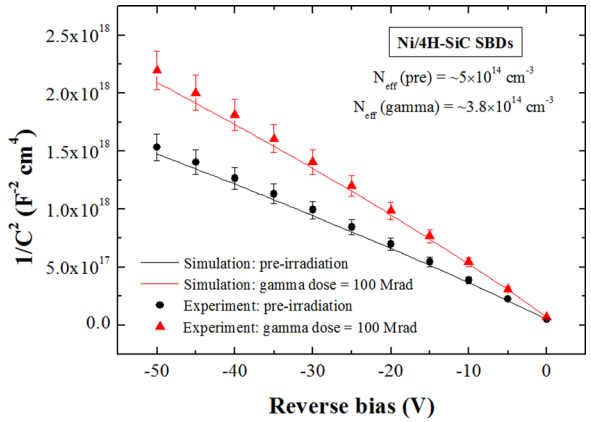

FIG. 12. Measured and simulated $(1/C^2)$-V characteristics of the Ni/4H-SiC SBDs before and after the ^{60}Co-gamma irradiation.

Hence, the gamma irradiation induced decrease in the effective doping concentration is the reason for the reduction in the E_m observed in Fig. 10, as per the Eq. (9).

The ^{60}Co-gamma irradiation effects on the $(1/C^2)$-V characteristics of the Ti/4H-SiC SBDs are displayed in Fig. 13. The effective doping concentration of the Ti/4H-SiC SBDs is decreased to $4.6 \times 10^{14}\,cm^{-3}$ after the gamma irradiation. Again, the gamma irradiation has less impact on change in the effective doping concentration of the Ti/4H-SiC SBDs because of the nonappearance of trap P2. Due to the presence of the deep level trap P2 with the concentration of $10^{14}\,cm^{-3}$, the electrical characteristics of the Ni/4H-SiC SBDs are considerably changed. Hence, as compared to Ni/4H-SiC SBDs, the Ti/4H-SiC SBDs have the better radiation tolerance for ^{60}Co-gamma rays at the dose of 100 Mrad. It is important to note that the simulation results are given a good agreement with the experimental data. So, the simulation studies may be extended for predicting the SBD electrical characteristics at higher gamma doses.[47]

V. CONCLUSION

The deep level defects in the epitaxial 4H-SiC SBDs have been identified before and after gamma irradiation by the TSCAP spectroscopy. Two electron traps at E_c-0.63 eV

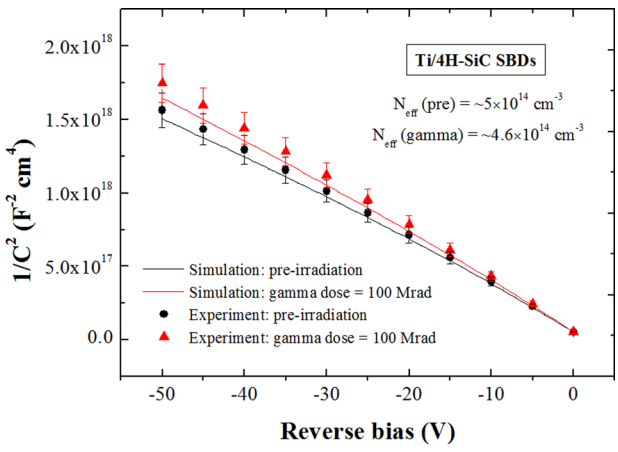

FIG. 13. Measured and simulated ^{60}Co-gamma irradiation induced changes in the $(1/C^2)$-V characteristics of the Ti/4H-SiC SBDs.

(P1), and E_c–1.13 eV (P2) are identified in the non-irradiated SBDs. One new trap at E_c–0.89 eV is found in the ^{60}Co-gamma irradiated SBDs at the dose of 100 Mrad, along with the traps P1, and P2 (with trap concentrations 10^{14} cm^{-3} in ranges). It is considered that the ^{60}Co-gamma irradiation produces intrinsic point defects in the n-type 4H-SiC epilayers and the electronic trap levels introduced within the bandgap by these intrinsic crystal defects are the acceptor-type traps. The dominant mechanisms responsible for the changes in the electrical characteristics after gamma irradiation are analyzed by using device simulations. The decrease in the effective doping concentration after gamma irradiation is due to the considerable increase in the concentration of acceptor-like defects. The gamma irradiation induced decrease in the leakage current density is mainly caused by the reduction in the tunneling current. As compared to Ni/4H-SiC SBDs, Ti/4H-SiC SBDs have better radiation resistance for ^{60}Co-gamma rays due to the absence of trap P2. Furthermore, it is noted that the simulated results closely track the measured post-irradiation characteristics of the SBDs at the dose of 100 Mrad. With the help of the extracted trap signatures, the radiation effects on the SBD characteristics at higher irradiation levels may be predicted.

ACKNOWLEDGMENTS

This work was partly supported by the Board of Research in Fusion Science and Technology (BRFST), India. We would like to thank Dr. Jamil Akhtar, CSIR-CEERI for his help during the fabrication. We also would like to thank Dr. Abhijit Saha, UGC-DAE CSR for his support in the gamma irradiation.

[1]See NASA Technical Report No. NASA/TM-2013-216516, E-18671, GRC-E-DAA-TN8288 (J. D. Wrbanek, S. Y. Wrbanek, and G. C. Fralick, Advanced Space Radiation Detector Technology Development, 2013).
[2]See NASA Technical Report No. 9342, Novel Silicon Carbide Deep Ultraviolet Detectors: Device Modeling, Characterization, Design and Prototyping Project, 2015.
[3]J. E. Lees, D. J. Bassford, E. J. Bunce, M. R. Sims, and A. B. Horsfall, Nucl. Instrum. Methods Phys. Res., Sect. A **604**, 174 (2009).
[4]F. Nava, A. Castaldini, A. Cavallini, P. Errani, and V. Cindro, IEEE Trans. Nucl. Sci. **53**, 2977 (2006).
[5]K. V. Nguyen, M. A. Mannan, and K. C. Mandal, IEEE Trans. Nucl. Sci. **62**, 3199 (2015).
[6]P. V. Raja, J. Akhtar, C. V. S. Rao, S. Vala, M. Abhangi, and N. V. L. N. Murty, Nucl. Instrum. Methods Phys. Res., Sect. A **869**, 118 (2017).
[7]P. V. Raja, J. Akhtar, S. Vala, M. Abhangi, and N. V. L. N. Murty, J. Instrum. **12**, P08006 (2017).
[8]M. C. E. Huber, A. Pauluhn, J. L. Culhane, J. G. Timothy, K. Wilhelm, and A. Zehnder, *Observing Photons in Space: A Guide to Experimental Space Astronomy* (Springer, New York, 2013).
[9]M. Bruzzi, IEEE Trans. Nucl. Sci. **48**, 960 (2001).
[10]T. Miyazaki, T. Makino, A. Takeyama, S. Onoda, T. Ohshima, Y. Tanaka, M. Kandori, T. Yoshie, and Y. Hijikata, Superlattices Microstruct. **99**, 197 (2016).
[11]P. G. Muzykov, R. M. Krishna, and K. C. Mandal, J. Appl. Phys. **111**, 014910 (2012).
[12]D. Menichelli, M. Scaringella, F. Moscatelli, M. Bruzzi, and R. Nipoti, Diamond Relat. Mater. **16**, 6 (2007).
[13]T. Dalibor, G. Pensl, H. Matsunami, T. Kimoto, W. J. Choyke, A. Schöner, and N. Nordell, Phys. Status Solidi A **162**, 199 (1997).
[14]J. Zhang, L. Storasta, J. P. Bergman, N. T. Son, and E. Janzén, J. Appl. Phys. **93**, 4708 (2003).
[15]I. Pintilie, L. Pintilie, K. Irmscher, and B. Thomas, Mater. Sci. Forum **433–436**, 463 (2003).
[16]K. Danno, T. Kimoto, and H. Matsunami, Appl. Phys. Lett. **86**, 122104 (2005).
[17]P. B. Klein, B. V. Shanabrook, S. W. Huh, A. Y. Polyakov, M. Skowronski, J. J. Sumakeris, and M. J. O'Loughlin, Appl. Phys. Lett. **88**, 052110 (2006).
[18]Ł. Gelczuk, M. Dabrowska-Szata, M. Sochacki, and J. Szmidt, Solid State Electron. **94**, 56 (2014).
[19]M. A. Mannan, S. K. Chaudhuri, K. V. Nguyen, and K. C. Mandal, J. Appl. Phys. **115**, 224504 (2014).
[20]M. A. Mannan, K. V. Nguyen, R. O. Pak, C. Oner, and K. C. Mandal, IEEE Trans. Nucl. Sci. **63**, 1083 (2016).
[21]C. Hemmingsson, N. T. Son, O. Kordina, J. P. Bergman, E. Janzén, J. L. Lindström, S. Savage, and N. Nordell, J. Appl. Phys. **81**, 6155 (1997).
[22]C. Hemmingsson, N. T. Son, O. Kordina, J. P. Bergman, E. Janzén, J. L. Lindström, S. Savage, and N. Nordell, Mater. Sci. Eng. B **46**, 336 (1997).
[23]A. Castaldini, A. Cavallini, L. Rigutti, F. Nava, S. Ferrero, and F. Giorgis, J. Appl. Phys. **98**, 053706 (2005).
[24]K. Danno and T. Kimoto, J. Appl. Phys. **101**, 103704 (2007).
[25]P. Hazdra, V. Zahlava, and J. Vobecky, Nucl. Instrum. Methods Phys. Res., Sect. B **327**, 124 (2014).
[26]P. V. Raja and N. V. L. Narasimha Murty, IEEE Trans. Nucl. Sci. **64**, 2377 (2017).
[27]I. Pintilie, L. Pintilie, M. Moll, E. Fretwurst, and G. Lindstroem, Appl. Phys. Lett. **78**, 550 (2001).
[28]C. T. Sah, W. W. Chan, H. S. Fu, and J. W. Walker, Appl. Phys. Lett. **20**, 193 (1972).
[29]G. L. Miller, D. V. Lang, and L. C. Kimerling, Annu. Rev. Mater. Sci. **7**, 377 (1977).
[30]D. V. Lang, *Thermally Stimulated Relaxation in Solids* (Springer, Berlin, Heidelberg, 1979), pp. 93–133.
[31]R. Joyce, K. Singh, S. Varghese, and J. Akhtar, Mater. Sci. Semicond. Process. **31**, 84 (2015).
[32]A. Kestle, S. P. Wilks, P. R. Dunstan, M. Pritchard, and P. A. Mawby, Electron. Lett. **36**, 267 (2000).
[33]L. Huang, B. Liu, Q. Zhu, S. Chen, M. Gao, F. Qin, and D. Wang, Appl. Phys. Lett. **100**, 263503 (2012).
[34]F. C. Beyer, C. Hemmingsson, H. Pedersen, A. Henry, J. Isoya, N. Morishita, T. Ohshima, and E. Janzén, Mater. Sci. Forum **679–680**, 249 (2011).
[35]F. C. Beyer, C. G. Hemmingsson, H. Pedersen, A. Henry, J. Isoya, N. Morishita, T. Ohshima, and E. Janzén, J. Phys. D: Appl. Phys. **45**, 455301 (2012).
[36]T. Kimoto and J. A. Cooper, *Fundamentals of Silicon Carbide Technology Growth, Characterization, Devices, and Applications* (John Wiley & Sons, Singapore, 2014).
[37]ATHENA Silvaco®, Silvaco's user guide, 2012.
[38]ATLAS Silvaco®, Silvaco's user guide, 2012.
[39]B. J. Baliga, *Silicon Carbide Power Devices* (World Scientific, Singapore, 2005), pp. 83–102.
[40]K. J. Schoen, J. M. Woodall, J. A. Cooper, and M. R. Melloch, IEEE Trans. Electron Devices **45**, 1595 (1998).
[41]S. M. Sze and K. K. Ng, *Physics of Semiconductor Devices* (John Wiley & Sons, New Jersey, 2007).
[42]L. Forbes and C. T. Sah, Solid State Electron. **14**, 182 (1971).
[43]M. Moll, Ph.D. thesis, Hamburg University, Hamburg, Germany, 1999.
[44]C. G. Hemmingsson, N. T. Son, A. Ellison, J. Zhang, and E. Janzen, Phys. Rev. B **58**, R10119 (1998).
[45]P. Carlsson, N. T. Son, F. C. Beyer, H. Pedersen, J. Isoya, N. Morishita, T. Ohshima, and E. Janzén, Phys. Status Solidi RRL **3**, 121 (2009).
[46]A. A. Lebedev, A. I. Veinger, D. V. Davydov, V. V. Kozlovski, N. S. Savkina, and A. M. Strel'chuk, J. Appl. Phys. **88**, 6265 (2000).
[47]P. V. Raja, C. V. S. Rao, and N. V. L. N. Murty, Nucl. Instrum. Methods Phys. Res., Sect. B **379**, 23 (2016).
[48]P. V. Raja, N. V. L. N. Murty, C. V. S. Rao, and M. Abhangi, J. Instrum. **10**, P10018 (2015).
[49]F. Nava, E. Vittone, P. Vanni, P. G. Fuochi, and C. Lanzieri, Nucl. Instrum. Methods Phys. Res., Sect. A **514**, 126 (2003).
[50]L. Zhang, C. Han, C. Y. J. Ma, Y. M. Zhang, and Y. M. Zhang, Acta. Phys. Sin. **58**, 2737 (2009); available at http://wulixb.iphy.ac.cn/EN/abstract/abstract15494.shtml.
[51]R. D. Harris, A. J. Frasca, and M. O. Patton, IEEE Trans. Nucl. Sci. **52**, 2408 (2005).